Low energy cluster deposition of nanoalloys

T. T. Järvi,[1,a)] A. Kuronen,[1] K. Nordlund,[1] and K. Albe[2]
[1]*Department of Physics, University of Helsinki, P.O. Box 43, Helsinki FI-00014, Finland*
[2]*Institut für Materialwissenschaft, Technische Universität Darmstadt, Petersenstr. 23, D-64287 Darmstadt, Germany*

(Received 22 June 2009; accepted 16 August 2009; published online 21 September 2009)

Low energy deposition of metal alloy nanoclusters is studied by molecular dynamics simulations. In a previous study, two mechanisms were introduced for epitaxial alignment of elemental clusters: The heating induced by the surface energy released upon impact and the thermally activated dislocation motion. In this study, these mechanisms are shown to dominate for Cu_3Ag, Cu_3Au, and Cu_3Ni clusters as well. The question whether the alloyed nature of the system or the initial chemical ordering of the particles influences epitaxial alignment with a substrate is discussed. Chemical ordering is shown to have a negligible effect due to disordering occurring at the initial stages of deposition. © *2009 American Institute of Physics*. [doi:10.1063/1.3225910]

I. INTRODUCTION

Manufacturing thin films is usually done by single-atom deposition methods.[1] An obvious additional degree of freedom to thin film deposition, the cluster size, is provided by cluster deposition.[2] Especially in cases where little damage to the substrate is desired, low energy cluster deposition may be a viable alternative to conventional methods since it allows high growth rates at low deposition rates.[3] Furthermore, nanocluster deposition provides a natural way to grow nanocrystalline films with well controlled grain sizes, as well as a method of assembling devices using deposition controlled by the adhesion properties of the substrate.[4] In the case of alloyed clusters, there is the additional degree of freedom of chemical composition that, for instance, provides an interesting possibility to manufacture thin films out of immiscible elements.[5] An extensive review of the physics of nanoalloys is provided in Ref. 6.

In a previous study,[7] we examined the epitaxial alignment of elemental metal clusters upon low energy deposition on a (100) surface of the same element. The maximum size of deposited clusters that align completely epitaxially on nanosecond time scales was determined, and two main mechanisms influencing epitaxiality were distinguished. First, the heating induced by the surface energy released on impact explained the cluster-size limit at low temperature. The temperature limit of superheating, or the mechanical melting point,[8–10] was found to be a critical quantity. That is, clusters that were sufficiently small to heat up to this temperature were able to recrystallize epitaxially. At high temperature, instead, the transient heating was overpowered by another mechanism, thermally activated dislocation motion. The nonepitaxial parts of deposited clusters are separated from the epitaxial ones by {111} twin boundaries,[7,11,12] the migration of which is caused by the motion of dislocations, finally leading to epitaxial clusters.

In this study, the above mechanisms are assessed for alloyed clusters. We will use three alloys, Cu_3Ag, Cu_3Au, and Cu_3Ni, as model systems. It is not obvious whether, or how, the alloyed nature of the clusters affects epitaxial alignment. We discuss the role of the miscibility of the alloyed elements and the initial chemical ordering. An important question is whether the initial chemical ordering of a cluster influences epitaxial alignment, either changing the mechanical melting or the dislocation mechanism. Also, ordered clusters can be expected to lose at least some of their internal order upon deposition,[13] but to our knowledge, a systematic cluster-size dependence has not been established. Furthermore, the change in short-range order provides a fingerprint of the processes occurring during deposition.

The effects operational on longer time scales, such as diffusion[14] and surface roughening,[15,16] can be expected to influence the final film structure; this is the first step in understanding the growth of alloyed films by cluster deposition.[17]

II. METHOD AND SIMULATIONS

Our simulation methods are explained in detail in our study of elemental clusters[7] and we give here only a brief summary.

We determined the limiting size of alloy clusters that align completely epitaxially upon thermal deposition on a (100) surface. The cluster and substrate were taken to consist of the same elements and to be at equal temperature, ranging from 0 to 750 K. For each case, namely, Cu_3Ag, Cu_3Au, and Cu_3Ni, the substrate was taken to be an $L1_2$-ordered lattice while the cluster atoms were distributed randomly. Note that even though two of the alloys used here are immiscible, the ordered phase was chosen as the substrate to eliminate the extra parameter of lattice mismatch.

The embedded-atom-method potentials[18] of Foiles *et al.*[19] were used to describe interatomic interactions. It must be emphasized that our goal is to clarify the atomic-scale mechanisms affecting epitaxial alignment. It should be noted that the potentials applied here do not exactly correspond to the respective elements in nature, as especially the stacking fault energies are significantly underestimated.

a)Electronic mail: tommi.t.jarvi@helsinki.fi.

The clusters were created as truncated octahedra and relaxed using the temperature control algorithm by Berendsen *et al.*[20] At all temperatures, most of the clusters remained as truncated octahedra upon relaxation, while the ones with icosahedral magic numbers relaxed to icosahedra. At high temperatures in the immiscible Cu_3Ag clusters, Ag, the component with larger atomic radius, showed a tendency to occupy surface sites.

After relaxation, the clusters were deposited with a translational energy of 25 meV/atom, chosen small enough not to play a role in epitaxial alignment. Clusters in the size range of 6–2000 atoms were deposited and their evolution was simulated for 2 ns. For each cluster size, roughly 20 simulations were performed to collect statistics. An individual cluster was judged epitaxial if there were no stable grains throughout the simulation. Thus if grains appeared and disappeared, the cluster was taken to be epitaxial.

To illustrate structural and short-range chemical order (SRO), two order parameters were used. To measure epitaxiality, the square of the structure factor[7]

$$S = \frac{1}{N}\sum_{i=1}^{N} e^{i\mathbf{k}\cdot\mathbf{r}_i} \tag{1}$$

of the cluster atoms was divided by that of the substrate atoms. Above, N is the number of atoms, with coordinate $\mathbf{r}_i$, and k is the wave vector $\mathbf{k}=2\pi(n_1,n_2,n_3)/a$ with the Miller index n_i and lattice constant a.

For SRO, we used the parameter

$$\mathrm{SRO} = 1 - \frac{n^A(B)}{n(B)c(A)}, \tag{2}$$

where $n^A(B)$ is the average number of A neighbors of atoms of type B, and $n(B)$ is their average total number of neighbors. $c(A)$ is the concentration of atoms of type A. For the present alloys, choosing, for example, for Cu_3Ag, both A and B as Ag, the order parameter is 1 for the $L1_2$-ordered phase and 0 for a random alloy.

III. RESULTS

The maximum size of clusters to reach complete epitaxy upon deposition is shown in Fig. 1. The upper error limit shows the next largest, nonepitaxial, cluster size. The left vertical axis shows the cube root of the number of atoms which serves as an effective radius for the clusters.

The main feature in Fig. 1 is the increase in the limit of epitaxy with temperature for all alloys. Moreover, at low temperatures, the limit is roughly the same for all the considered alloys, while at 750 K, there is a difference of a factor of roughly 3 in the limit of epitaxy between the lowest limit for Cu_3Ni and the highest for Cu_3Au. This behavior is in agreement with the one observed previously for elemental clusters.[7,21,22]

In the following, we will first address the effect of chemical order on epitaxial alignment and then discuss the results in two parts: first, considering the low-temperature behavior and, second, the high-temperature behavior of the limit. Finally, we combine the models to explain our simulation results.

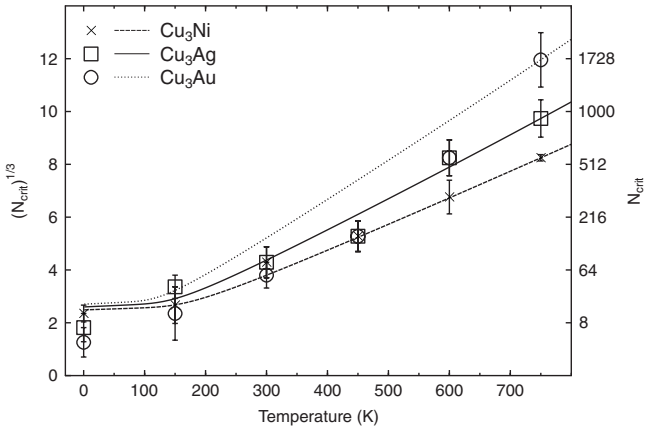

FIG. 1. Maximum size, N_{crit} (i.e., number of atoms), of alloy clusters that align completely epitaxially upon deposition. The curves show the predictions of the combined model discussed in Sec. III D.

A. Effect of chemical order on epitaxial alignment

An important question is whether the initial chemical ordering of a cluster influences epitaxial alignment. This mainly concerns the larger clusters as clusters with sizes relevant to low-temperature epitaxy are too small to have significant differences in chemical ordering.

Ordered clusters can be expected to lose at least some of their internal orders upon deposition.[13] Figure 2 shows the time evolution of the short-range order parameter for 976 atom Cu_3Ag clusters, both relaxed starting from a random alloy, as explained above, and $L1_2$-ordered ones. The curves have been averaged over several simulation runs. As expected, there is little change in the order parameter of the random alloy particles during deposition. The $L1_2$-ordered clusters, however, experience significant disordering, reaching a value of the order parameter comparable to that of the randomly alloyed clusters.

Figure 2 also shows the normalized structure factors of the clusters. Contrary to the short-range order, the epitaxiality keeps increasing after the initial impact, indicating that while the decrease in chemical order happens in the begin-

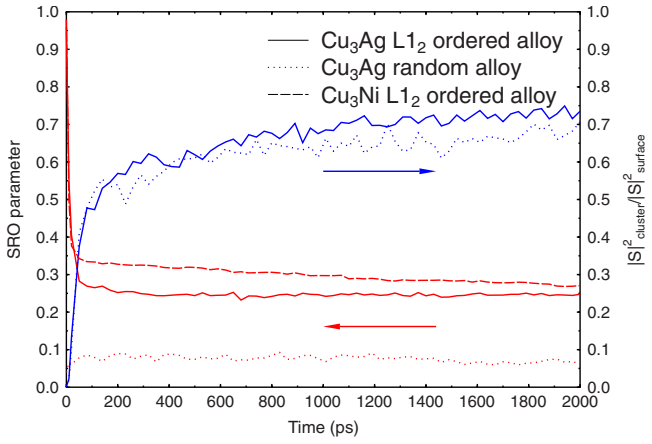

FIG. 2. (Color online) Short-range order parameter and normalized structure factor for 976 atom Cu_3Ag and Cu_3Ni clusters during deposition at 750 K. The curves are averages over several simulation runs. A value of SRO=1 corresponds to an $L1_2$-ordered system, while a random alloy gives SRO=0.

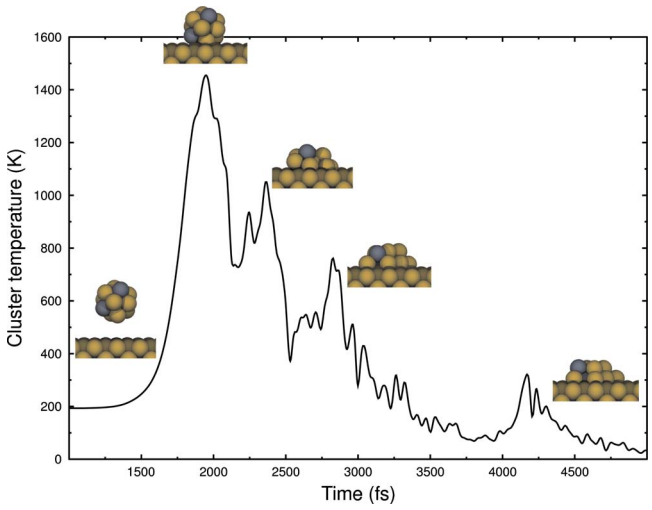

FIG. 3. (Color online) Temperature of a 13 atom Cu_3Ni cluster during deposition. The snapshots show the cluster at various times, with yellow atoms being Cu.

ning of the deposition process, epitaxial alignment also occurs later on. The chemical order thus seems to decrease by the exchange of atoms between lattice sites as the cluster lands on the surface, as observed previously.[13]

This behavior was found to be common to Cu_3Ag and Cu_3Au. For Cu_3Ni instead, also the short-range order kept decreasing slowly but steadily throughout the simulations, as shown in Fig. 2. Furthermore, the decline was steady in individual simulations as well, as opposed to epitaxiality that tends to increase in sudden jumps. This suggests that the evolution of the order parameters is governed by different processes. As discussed in detail later on, epitaxiality increases (at large time scales) by dislocation processes while short-range order can, in the present system, be assumed to evolve mainly through surface diffusion. The reason why Cu_3Ni is the only alloy where chemical disordering continues at long time scales is that for it, a random alloy is energetically more favorable by roughly 4 meV/atom, while for the other alloys, the energetics favors the ordered phase by $\sim$10–20 meV/atom. Finally, for all the alloys considered, the epitaxiality shows no significant dependence on the clusters' initial chemical ordering.

We will return to the mechanism by which chemical disordering occurs but we will first discuss the way in which epitaxial alignment is achieved at the lower temperatures.

B. Epitaxial alignment at low temperature

As a cluster is deposited on the surface, the released surface energy heats it. This happens on a picosecond time scale, as shown for a 13 atom Cu_3Ni cluster in Fig. 3. The cluster cools down to the ambient temperature very rapidly. After this, in the case of high temperature, thermal evolution takes place.

In Ref. 7, we calculated the maximum size of a cluster that melts by this initial heating. Assuming that the cluster is spherical in shape, and that the surface energy heating the cluster is released from an area of twice the area of a segment of a sphere, we calculated the maximum size of a cluster to reach a certain temperature, T_{melt}. The height of the segment, h, was taken equal to one lattice constant, a.

TABLE I. Barriers $\gamma_{\mathrm{UTB}}-\gamma_{\mathrm{TB}}$ for twin boundary migration and the main properties of the alloys of Foiles *et al.* (Ref. 19) used in the present study. The properties are the superheating melting point, $T_{\mathrm{melt}}^{\mathrm{SH}}$, for a random alloy and the (100) surface energy $\gamma_{\{100\}}$ for the $L1_2$-ordered surface with only copper atoms in the top monolayer.

	Cu_3Ni	Cu_3Ag	Cu_3Au
$T_{\mathrm{melt}}^{\mathrm{SH}}$ (K)	1655	1310	1278
$\gamma_{\{100\}}$ (J/m^2)	1.34	1.07	1.12
$\gamma_{\mathrm{UTB}}-\gamma_{\mathrm{TB}}$ (mJ/m^2)	152	117	99

The critical cluster radius is then given by

$$r_{\mathrm{crit}} = \sqrt{\frac{\gamma h a^3}{4k_B\beta}}\frac{1}{\sqrt{T_{\mathrm{melt}}-T_i}}, \tag{3}$$

where γ is the surface energy and β is a factor that corresponds to the fraction of released surface energy transferred to the cluster. We take β equal to 2, corresponding to half the energy to the cluster and half to the substrate. Finally, T_i is the initial cluster (and substrate) temperature. Note that the above formula is derived without any fitted parameters.

It is well known that the melting of nanoparticles differs significantly from bulk melting.[23] In the case of cluster deposition, the heating induced by the released surface energy dissipates very fast, in only a few picoseconds. Hence, thermodynamic melting, which is a nucleation-and-growth process, can be questioned as the relevant mechanism. Instead, the temperature limit of superheating, or the mechanical melting point,[8–10,24,25] can be used as a measure of the stability of the fcc lattice of the cluster. This temperature is about 15%–20% above the bulk thermodynamic melting point,[8,10] the values for the potentials of the present study being given in Table I. They have been determined simply by simulating a bulk system with periodic boundary conditions and by examining at which temperature homogeneous melting occurs.

The critical cluster sizes at 0 K predicted by Eq. (3) are about 15, 18, and 20 for Cu_3Ni, Cu_3Ag, and Cu_3Au, respectively. These are only slightly larger than the values obtained from the simulations. Taking into account the simplified nature of the model, and the fact that it has no fitted parameters, the correspondence is very good. The model also explains why the differences in the low-temperature limit of epitaxy between the elements are small. Note also that in the case of energetic deposition of nanoparticles of thousands of atoms, the above model has been shown to predict the energy needed for epitaxial deposition quite accurately.[26]

C. Chemical disordering during deposition

We shall now return to the chemical disordering occurring in the initial stages of deposition. The size dependence of the extent to which the particles are disordered turns out to be interesting. Figure 4 shows the fraction of atoms that are disordered when $L1_2$-ordered Cu_3Ag particles of different sizes are deposited at 300 K. (The number of disordered atoms was defined as the number of Ag atoms that had Ag

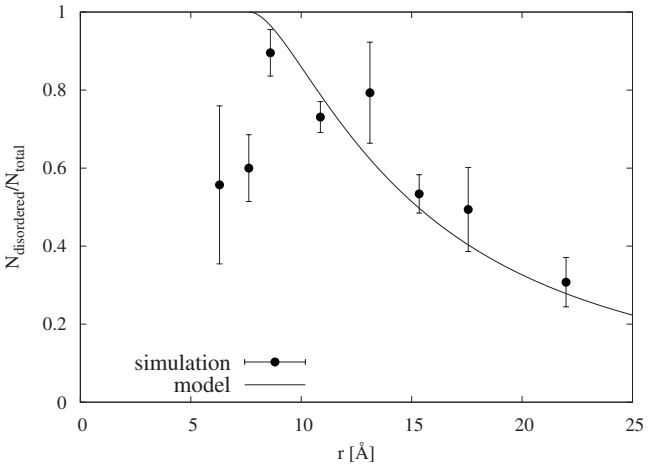

FIG. 4. The fraction of atoms that are disordered when $L1_2$-ordered Cu_3Ag particles are deposited at 300 K, as a function of cluster radius. The line is a fit to the model described in Sec. III C.

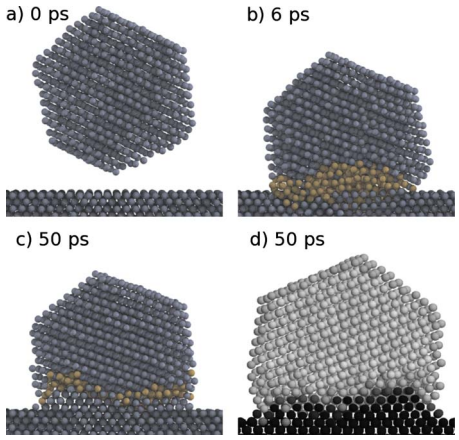

FIG. 5. (Color online) Deposition of a Cu_3Ag particle of 22 Å radius at 300 K. In (a)–(c), disordered (liquidlike) atoms are colored yellow/light and crystalline ones blue/dark. (d) is in a different orientation from (a)–(c) and the coloring is based on the degree of epitaxy, the darker atoms being more epitaxial.

neighbors, scaled with the Ag concentration.) From a plot of the number of disordered atoms versus cluster size (not shown), it is clear that there is a linear relationship between the number of disordered atoms and the cluster radius.

We tried to explain the disordered fraction based on the mechanical melting model but unfortunately the model turned out to be too simplistic for that. Ignoring thermal conduction effects, for example, is clearly not a good approximation for the larger particles.

The results can be rationalized with a simple assumption, though. If one assumes that the clusters are spherical in shape and that the atoms that are disordered are in a segment of height h from the bottom of the sphere in contact with the substrate, one gets the relationship

$$\frac{N_{\text{disordered}}}{N_{\text{total}}} = \frac{3h^2}{4r^3}\left(r - \frac{h}{3}\right), \tag{4}$$

where r is the radius of the cluster. This expression only has one parameter to be fitted, namely, the segment height h. Fitting the value to the simulation data gives $h \approx 15$ Å, the resulting line being shown in Fig. 4. Note that for $r < h/2$, that is, for the two smallest cluster sizes, the expression is an extrapolation as the geometric model loses its meaning. What is also interesting is that, for the cluster sizes relevant to determining the size limit of complete epitaxy, the disordering is extensive, and thus choosing random initial chemical ordering for the clusters used to determine the limits in Fig. 1 is justified.

The geometry is best displayed in the larger particles. Figures 5(a)–5(c) show the deposition of a cluster of 22 Å radius (3355 atoms) with the atoms colored according to an algorithm based on bond correlation using spherical harmonics,[27] enabling the separation of disordered (liquidlike, yellow/light) and crystalline (blue/dark) atoms. Figure 5(d) shows the final configuration with the atoms colored according to their degree of epitaxy, which was determined using the method described in Ref. 21. It is apparent that chemical disordering is linked to the configurational disorder occurring during deposition and is driven by the formation of a contact epitaxial layer, which is clearly visible in Fig. 5(d). For the smaller particles, approaching the completely epitaxial cluster sizes, the thickness of the epitaxial layer approaches the cluster diameter, thus leading to completely disordered clusters.

D. Epitaxial alignment at high temperature

We now turn to discuss the high-temperature behavior of the limit of epitaxy, which cannot be explained by the melting model. At 750 K there is a difference of a factor of roughly 3 in the limit between Cu_3Ni and Cu_3Au. This behavior can be explained by the mechanism of twin boundary migration, introduced in Ref. 7.

Figure 6 shows snapshots of the evolution of a 405 atom Cu_3Ni particle after deposition at 600 K. Initially, 50 ps after deposition, the particle has two twinned regions, both two {111} layers in thickness. This property, that the nonepitaxial parts of the clusters are almost exclusively accommodated to the epitaxial part by {111} twin boundaries, is typical for fcc metals.[7,11,21,22] During the simulation, dislocations glide through the twin boundaries, causing the boundaries to migrate. In this particular case, the particle was judged epitaxial as there were no stable twinned regions present.

The above process of twin boundary migration is thermally activated and can be shown to determine the maximum size of epitaxial clusters.[7] Since a moving partial dislocation introduces a local stacking fault, the barrier associated with its motion is determined by the difference between the stable (γ_{TB}) and the unstable (γ_{UTB}) twinning fault position. The barrier was determined as described in our earlier work,[7] averaging the results over several runs with independently generated random alloy configurations. It must be emphasized that because of the initial chemical disordering of ordered alloy clusters upon deposition, described in Sec. III A, this is a very reasonable approximation.

The barrier $\gamma_{\text{UTB}} - \gamma_{\text{TB}}$ determines the activation energy, E_{activ}, which a Shockley partial of length l has to surmount to move a distance of $b = a/\sqrt{6}$ to the next local minimum:

$$E_{\text{activ}} = (\gamma_{\text{UTB}} - \gamma_{\text{TB}})bl. \tag{5}$$

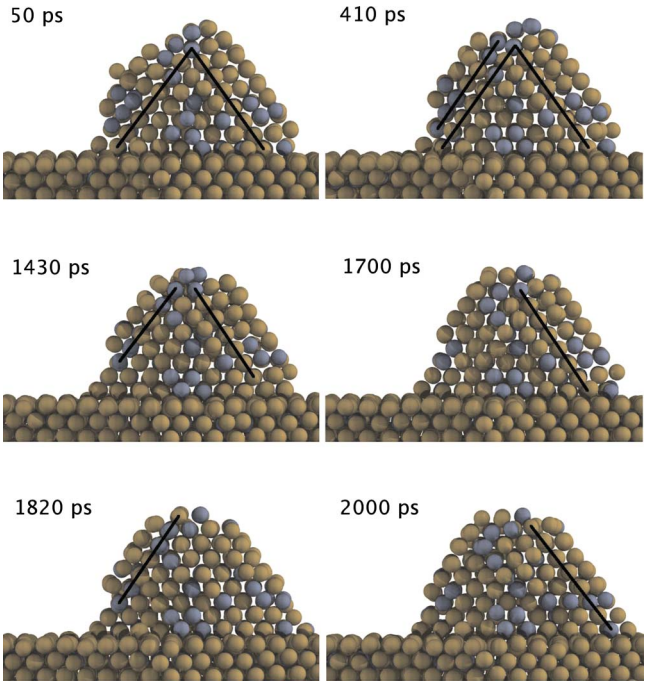

FIG. 6. (Color online) Snapshots of the evolution of a 405 atom Cu_3Ni particle after deposition at 600 K. Twinned regions appear and disappear with time. Lines have been drawn at the twin boundaries. The yellow atoms are Cu.

The length of the dislocation line depends on the cluster size and can, as a first approximation, be taken as the diameter of the cluster. It must be emphasized that this definition makes the activation energy dependent on the cluster size.

In our earlier study,[7] we showed that for the critical cluster sizes, one has the relation

$$n = \frac{r}{d_{\{111\}}} \propto t\nu_D l e^{-E_{\mathrm{activ}}(N_{\mathrm{crit}})/k_B T}, \tag{6}$$

where $n = r/d_{\{111\}}$ is the number of {111} layers that have to be turned epitaxial by the dislocation motion. t is the simulation time (2 ns) and ν_D is the Debye frequency. (The Debye frequencies were calculated from Debye temperatures that were approximated with a weighted average of the elements' values.)

As the simulation time is constant and $l = 2r$, one gets

$$e^{-E_{\mathrm{activ}}(N_{\mathrm{crit}})/k_B T} \propto \frac{1}{d_{\{111\}}\nu_D} \approx \mathrm{const} \tag{7}$$

for the critical cluster sizes N_{crit}. The factor $1/d_{\{111\}}\nu_D$ is constant within ~20% between the alloys.

Based on Eq. (7), the activation energy has to be the same for the alloys at the critical cluster size. Indeed, using Eq. (5), and the critical cluster sizes, to estimate the activation energy for the different alloys at 750 K, gives the values shown in Fig. 7. These are all close to 0.3 eV. Figure 7 also shows the values for elemental metal clusters, determined in Ref. 7. The inset shows the correlation between the barrier $\gamma_{\mathrm{UTB}} - \gamma_{\mathrm{TB}}$ and the critical cluster size.

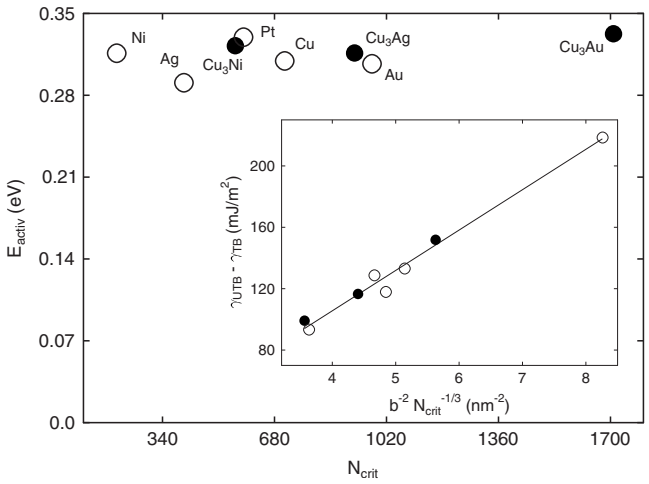

FIG. 7. Activation energy for thermal motion of twinning dislocations in clusters of critical size N_{crit} at 750 K. The inset shows the linear correlation between the barrier $\gamma_{\mathrm{UTB}} - \gamma_{\mathrm{TB}}$ and the critical cluster size. The filled circles correspond to the present alloy results while the hollow ones give the elemental metal data (for Cu, Ag, Au, Ni, and Pt) according to Ref. 7.

This is a strong indication that the thermally activated dislocation motion mechanism is the correct explanation for the differences in epitaxial alignment between different alloys and elements at high temperature.

Combining the two models into a single expression for the limit of epitaxy is not straightforward. In the intermediate temperature range, the combined expression should always give limits larger or equal to the individual models, while reducing to them at the extremes. To accomplish this, we modify the left-hand side of Eq. (6) to read $(r - r_{\mathrm{mm}})/d_{\{111\}}$, where r_{mm} is the critical cluster radius given by the melting model in Eq. (3). Thus, at the limit where the critical cluster size r is much larger than r_{mm}, the melting model is insignificant, whereas for small clusters it sets a lower limit for r. Absorbing the (material dependent) constants in a single factor C gives

$$e^{-E_{\mathrm{activ}}(r_{\mathrm{crit}})/k_B T} = C\left(1 - \frac{r_{\mathrm{mm}}}{r_{\mathrm{crit}}}\right), \tag{8}$$

where $E_{\mathrm{activ}}(r_{\mathrm{crit}})$ is defined by Eq. (5) with $l = 2r$.

The factor C, for each alloy, can be determined from the simulation results at a given temperature, say, 750 K. Solving Eq. (8) for r_{crit} numerically gives the curves shown in Fig. 1 with the simulation results. All the high-temperature data fall on the curves nicely. Only for Cu_3Au is the match for some reason less perfect.

The high-temperature dependence of the limit of epitaxy obtained from simulation is linear. Indeed, it can be obtained by noting that from Eq. (7) it follows that the fraction E_{activ}/T is constant. From Eq. (5), it then follows that $N_{\mathrm{crit}}^{1/3} \propto T$.

IV. DISCUSSION

Our present results give further support to the mechanisms of thermally activated dislocation motion and initial mechanical melting in epitaxial alignment. While other mechanisms cannot be completely ruled out, it seems that

these two are the most important ones. Evidence to support this has also been found for heteroepitaxial deposition of Co on Cu(100) in Ref. 28.

We also show that the alloyed nature of the deposited particles does not influence the mechanisms of epitaxial alignment significantly. Furthermore, the effect of the clusters' initial chemical ordering is negligible due to disordering occurring at the initial stages of deposition.

Finally, the capability of molecular dynamics simulations limits the accessible time scales, and the simulation time of the present study is 2 ns. On deposition of cluster assembled films, also surface roughness affects the final state[15,16] and adatom migration[14] is expected to work toward turning the cluster into a single monolayer. Also mixing with the substrate may occur on longer time scales.[29]

Knowing the mechanisms of initial epitaxial reorganization is the key to understand the subsequent evolution of deposited nanoparticles. However, further studies on long time-scale effects and the formation of cluster assembled films are required.

V. CONCLUSIONS

The mechanisms of epitaxial alignment are the same in the case of alloys as with elemental clusters. In the case of alloys, disordering occurs in the initial stage of deposition. We show that the extent of disordering can be rationalized in a simple geometrical model. The results indicate that cluster-deposited films will be disordered at least at small grain sizes. We further unite the models describing low- and high-temperature epitaxial alignments into a single expression, thus clarifying the relationship between the two.

ACKNOWLEDGMENTS

This work was performed within the Finnish Centre of Excellence in Computational Molecular Science (CMS), financed by the Academy of Finland and the University of Helsinki. It was supported by the Academy of Finland under Project No. 205729. We also gratefully acknowledge support within an exchange program from the Academy of Finland and the German Foreign Exchange Service (DAAD), as well as the grants of computer time from CSC, the Finnish IT Center for Science.

[1] J. A. Venables, *Introduction to Surface and Thin Film Processes* (Cambridge University Press, Cambridge, 2000).
[2] P. Melinon, V. Paillard, V. Dupuis, A. Perez, P. Jensen, A. Hoareau, J. P. Perez, J. Tuaillon, M. Broyer, J. L. Vialle, M. Pellarin, B. Baguenard, and J. Lerme, Int. J. Mod. Phys. B **9**, 339 (1995).
[3] I. Yamada, J. Matsuo, N. Toyoda, and A. Kirkpatrick, Mater. Sci. Eng., R. **34**, 231 (2001).
[4] R. Reichel, J. G. Partridge, F. Natali, T. Matthewson, S. A. Brown, A. Lassesson, D. M. A. Mackenzie, A. I. Ayesh, K. C. Tee, A. Awasthi, and S. C. Hendy, Appl. Phys. Lett. **89**, 213105 (2006).
[5] E. D. Tober, R. F. C. Farrow, R. F. Marks, G. Witte, K. Kalki, and D. D. Chambliss, Phys. Rev. Lett. **81**, 1897 (1998).
[6] R. Ferrando, J. Jellinek, and R. L. Johnston, Chem. Rev. (Washington, DC) **108**, 845 (2008).
[7] T. T. Järvi, A. Kuronen, K. Meinander, K. Albe, and K. Nordlund, Phys. Rev. B **75**, 115422 (2007).
[8] R. W. Cahn, Nature (London) **413**, 582 (2001).
[9] M. Forsblom and G. Grimvall, Nature Mater. **4**, 388 (2005).
[10] F. Delogu, Mater. Sci. Eng., A **403**, 48 (2005).
[11] M. Hou, Nucl. Instrum. Methods Phys. Res. B **135**, 501 (1998).
[12] S.-C. Lee, B. D. Yu, D.-Y. Kim, and N. M. Hwang, J. Cryst. Growth **242**, 463 (2002).
[13] V. S. Kharlamov, E. E. Zhurkin, and M. Hou, Nucl. Instrum. Methods Phys. Res. B **193**, 538 (2002).
[14] J. Frantz, M. Rusanen, K. Nordlund, and I. T. Koponen, J. Phys.: Condens. Matter **16**, 2995 (2004).
[15] K. Meinander, K. Nordlund, and J. Keinonen, Nucl. Instrum. Methods Phys. Res. B **228**, 69 (2005).
[16] K. Meinander, T. T. Järvi, and K. Nordlund, Appl. Phys. Lett. **89**, 253109 (2006).
[17] M. Hou, V. S. Kharlamov, and E. E. Zhurkin, Phys. Rev. B **66**, 195408 (2002).
[18] M. S. Daw and M. I. Baskes, Phys. Rev. B **29**, 6443 (1984).
[19] S. M. Foiles, M. I. Baskes, and M. S. Daw, Phys. Rev. B **33**, 7983 (1986).
[20] H. J. C. Berendsen, J. P. M. Postma, W. F. van Gunsteren, and J. R. Haak, J. Chem. Phys. **81**, 3684 (1984).
[21] K. Meinander, J. Frantz, K. Nordlund, and J. Keinonen, Thin Solid Films **425**, 297 (2003).
[22] K. Meinander, personal communication (2006). The temperature scale of Fig. 5 in Ref. 21 has to be rescaled by a factor of $\frac{36}{25}$.
[23] F. Baletto and R. Ferrando, Rev. Mod. Phys. **77**, 371 (2005).
[24] A. V. Granato, Phys. Rev. Lett. **68**, 974 (1992).
[25] K. Nordlund and R. S. Averback, in *Defect and Diffusion in Metals—Annual Retrospective 2000*, edited by D. J. Fisher (Scitec, Zürich, Switzerland, 2000).
[26] K. Nordlund, T. T. Järvi, K. Meinander, and J. Samela, Appl. Phys. A: Mater. Sci. Process. **91**, 561 (2008).
[27] E. Mendez-Villuendas and R. K. Bowles, Phys. Rev. Lett. **98**, 185503 (2007).
[28] J. C. Jiménez-Sáez, A. M. C. Pérez-Martín, and J. J. Jiménez-Rodríguez, Phys. Status Solidi A **205**, 1330 (2008).
[29] D. N. Tafen and L. J. Lewis, Phys. Rev. B **77**, 075429 (2008).